Identification of the origin of radiocesium released into the environment in areas remote from nuclear accident and military test sites using the $^{135}Cs/^{137}Cs$ isotopic signature

Anaelle Magre, Beatrice Boulet, Anne de Vismes Ott, Olivier Evrard, Laurent Pourcelot

Identification of the origin of radiocesium released into the environment in areas remote from nuclear accident and military test sites using the $^{135}Cs/^{137}Cs$ isotopic signature

Anaelle Magre [a,b], Beatrice Boulet [a], Anne de Vismes [a], Olivier Evrard [b], Laurent Pourcelot [c]*

[a] Laboratoire de métrologie de la radioactivité dans l'environnement (PSE-ENV/SAME/LMRE), IRSN, 91400 Orsay, France

[b] Laboratoire des Sciences du Climat et de l'Environnement (CNRS, CEA, UVSQ-IPSL), Université Paris-Saclay, 91191 Gif-sur-Yvette, France

[c] Laboratoire d'étude et d'expertise sur la radioactivité de l'environnement (PSE-ENV/SEREN/LEREN), IRSN, 13108 Saint-Paul-lez-Durance, France

[*]*Corresponding author: laurent.pourcelot@irsn.fr, Bât. 153. – BP 1, 13108 Saint-Paul-Lez-Durance (France)*

Abstract

The isotopic signature of radionuclides provides a powerful tool for discriminating radioactive contamination sources and estimating their respective contributions in the environment. In this context, the $^{135}Cs/^{137}Cs$ ratio has been tested as a very promising isotopic ratio that had not been explored yet in many countries around the world including France. To quantify the levels of radioactivity found in the environment, a new method combining a thorough radiochemical treatment of the sample and an efficient measurement by ICP-MS/MS has been recently developed. This method was successfully applied, for the first time, to soil and sediment samples collected in France in two mountainous regions preferentially impacted either by global fallout from nuclear weapons testing (*i.e.,* the Pyrenees) or by the Chernobyl accident (*i.e.,* the Southern Alps). The $^{135}Cs/^{137}Cs$ ratios measured on twenty-one samples ranged from 0.66 ± 0.04 and 4.29 ± 0.21 (decay-corrected to January 1st, 2022) corresponding to the characteristic signatures of the fallout from Chernobyl and global fallout associated with the nuclear weapons testing, respectively. Moreover, large variations of both the ^{137}Cs mass activity and the studied isotopic ratio recorded by most samples from the southern Alps suggest varying proportions of these two ^{137}Cs sources. For these samples, the contribution of each source was estimated using this new tracer ($^{135}Cs/^{137}Cs$) and compared with the mixing contribution given by activity ratio: $^{239+240}Pu/^{137}Cs$. This work has successfully demonstrated the applicability of the $^{135}Cs/^{137}Cs$ isotopic signature to nuclear forensic studies and could be extended to better evaluate the environmental impact of nuclear facilities (*i.e.,* NPP, waste reprocessing).

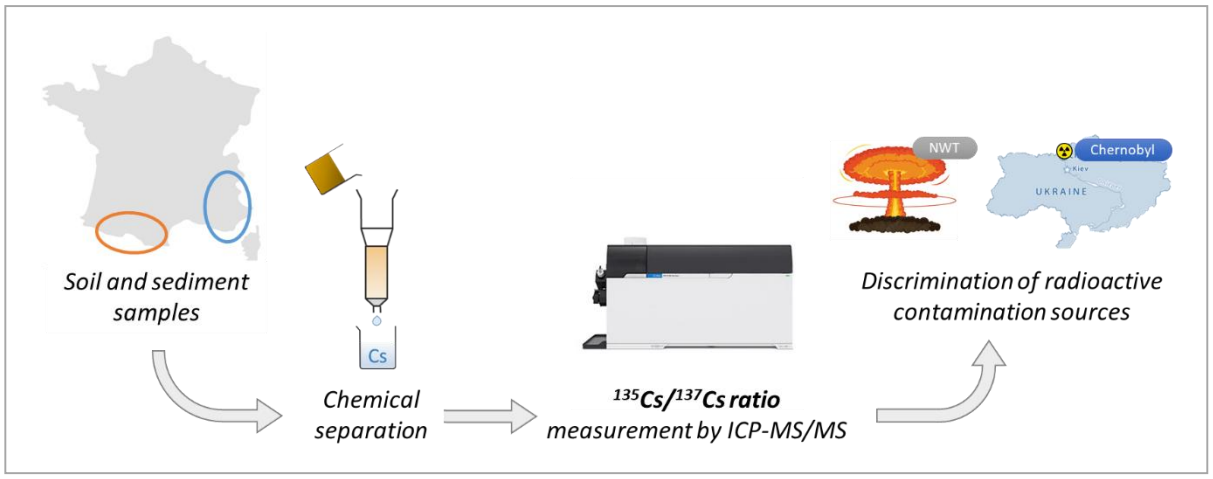

Keywords

Environmental monitoring, radioactive contamination, isotopic signatures, ICP-MS/MS

Introduction

Since the 1950s, nuclear activities have been undertaken to develop medical, industrial, energy or military applications[1]. These activities resulted in radioactive releases of about 8.1×10^{20} Bq[2,3]. Radiocesium isotopes including ^{134}Cs ($T_{1/2}$ = 2.1 y), ^{135}Cs ($T_{1/2}$ = $2.3.10^6$ y) and ^{137}Cs ($T_{1/2}$ = 30.2 y) rank among the radionuclides that were released in highest quantities [4,5]. With more than 1.4×10^8 Bq dispersed into the environment and its relatively long half-life, ^{137}Cs is considered as the main source of long-term artificial radiation to the public[4–8]. Its monitoring in the environment is therefore of major interest to evaluate the risks incurred by the population and ecosystems [9–12]. It is therefore essential to be able to identify unambiguously the origin of radioactive contamination and to anticipate their potential impacts. Three main radioactive contamination sources of ^{137}Cs are distinguished in the environment, even if the proportion of each varies from an environmental sample to another. Thus ^{137}Cs may result from nuclear weapons testing (NWT), nuclear power plant accidents (Chernobyl in 1986 and Fukushima in 2011) and authorized discharges from nuclear facilities[2,13–15].

^{137}Cs is easily measured by gamma-ray spectrometry[7,16,17]. However, due to its potential supply from contrasted sources and its accumulation in the environment for several decades, its measurement alone does not allow to identify the origin of this contamination. To discriminate it, a method has been proposed based on the occurrence of contrasted isotopic signatures between the different radiocesium sources[18–20]. The isotopic ratios are commonly employed to understand the mechanisms of release, transport, or redistribution of radionuclides in the environment. Knowledge of radionuclide signatures is also of major interest for characterizing the radiological background to assess the specific contribution of potential future contamination events. In this context, several ratios have been employed to identify and characterize ^{137}Cs sources in the environment such as the $^{239+240}Pu/^{137}Cs$ activity ratio[21–26]. Nevertheless, the hypothesis of fractionation of two elements (Pu and Cs) with different bio-geochemical properties could not be excluded. As an alternative, the radiocesium isotopic signature was also used for many years by directly measuring the $^{134}Cs/^{137}Cs$ ratio by gamma-ray spectrometry[15,17,27–30]. However, the use of this ratio is limited to a period of maximum ten years following the release due to the relatively short half-life of ^{134}Cs, a radionuclide that is no longer detectable in areas lowly affected by Fukushima fallout[12,31,32]. In this context, an alternative was recently proposed by analyzing the much longer-lived ^{135}Cs ($T_{1/2}$ = $2.3.10^6$ y). The discriminating power of the $^{135}Cs/^{137}Cs$ isotopic ratio was demonstrated in several studies, which aims at identifying nuclear contamination sources and for

improving our understanding of the dispersion patterns of anthropogenic radionuclides[1,20,32–34]. The characteristic $^{135}Cs/^{137}Cs$ atomic ratios reported in the literature for fallout from the NWT, the Chernobyl accident and the Fukushima accident were 3.70 ± 0.68[32,35], 0.66 ± 0.03[1,20,32,36,37] and 0.45 ± 0.02[12,33,36,38] (decay-corrected to January 1st, 2022), respectively. Nevertheless, it is noteworthy that very few data were reported for the NWT.

Despite the potential usefulness of the $^{135}Cs/^{137}Cs$ ratio, few data are available in environmental samples collected away from exclusion zones and former nuclear testing areas, due to several analytical challenges associated with the ^{135}Cs quantification[39,40]. Its measurement was previously extremely difficult, if not impossible, by the use of radiometric methods because of the ^{135}Cs low-beta emissions (β^-, E_{max} 268.9 keV)[33,41]. The most suitable measurement technique for ^{135}Cs is therefore mass spectrometry[42] such as ICP-MS/MS, first commercialized in 2013 by Agilent, requiring a specific sample treatment[12,32,43]. However, in the environment and in zones that were not exposed to accidental or military radionuclide releases, only a low amount of radiocesium is available, while much higher levels of several elements causing spectral interferences at m/z 135 and 137 (^{135}Ba, ^{137}Ba, $^{95}Mo^{40}Ar$, $^{97}Mo^{40}Ar$, $^{119}Sn^{16}O$, $^{121}Sb^{16}O$) are found [44]. To overcome these difficulties, a high Cs-selective radiochemistry procedure must be applied to a large quantity of sample (resulting in complex chemistry) and it must be combined with an efficient mass spectrometry measurement to remove any trace of interferents before the quantification of the $^{135}Cs/^{137}Cs$ isotopic ratio[12,32,36,37].

The goal of the current research was therefore to investigate the applicability of the $^{135}Cs/^{137}Cs$ isotopic signature for identifying contrasted ^{137}Cs sources and estimating their respective contributions to radiocesium found in environmental samples collected in an area remote from nuclear accident and test sites (*i.e.,* mainland France). To achieve this objective, twenty-one soil or sediment samples (matrices known to strongly absorb ^{137}Cs by clay minerals) were collected in two main regions preferentially impacted by either fallout from atmospheric nuclear weapons tests, the Chernobyl accident or both sources[21,23]. Indeed,^{137}Cs deposited in France soon after the releases from the Fukushima accident is considered to be negligible in comparison with ^{137}Cs from Chernobyl accident (500 to more than 1000 lower levels)[45]. The $^{135}Cs/^{137}Cs$ isotopic ratio were then quantified by ICP-MS/MS after extracting and purifying the cesium from the solid matrix according to the method recently proposed by Magré et al. (2022)[43].

The data obtained on the soils and sediments samples taken in France were then used to estimate the contribution of each source by comparing the original $^{135}Cs/^{137}Cs$ ratios determined in this

research with the characteristic ratios of ^{137}Cs sources reported in the literature. In addition, the proportion of each source estimated with this new tracer ($^{135}Cs/^{137}Cs$) was compared with those given by other more commonly used diagnostic ratios such as $^{239+240}Pu/^{137}Cs$.

Experimental section

Environmental samples.

Soils and sediments collected in France. The selection of environmental samples was based on previous work namely the cartographic reconstruction of the ^{137}Cs theorical deposits in France following NWT or the Chernobyl accident. To characterize the fallout from each of these ^{137}Cs sources, samples from two regions preferentially impacted by either NWT or Chernobyl fallout were studied. The investigated areas are respectively located in the mountainous areas of Pyrenees and in the Mercantour (southern French Alps), both regions being devoid of any nuclear facility, so that NWT and Chernobyl fallout provide the only sources of artificial radioactivity. The environmental matrices analyzed were soils and lake sediments, and they were chosen because of their strong capacity to fix radiocesium onto clay minerals. Indeed, in these matrices, ^{137}Cs activities ranged from a few $Bq.kg^{-1}$ to a few tens of $Bq.kg^{-1}$ and could reach several thousands of $Bq.kg^{-1}$ in mountainous areas[46,47].

In this study, ten lake sediment, four surface soil (0-5 cm depth) and three subsurface soil (5-10 cm depth) samples collected in the Mercantour massif between 2013 and 2021 were analyzed (Figure 1). Four soil samples collected in 2014 in the Pyrenees were also investigated, including three surface soils (0-10 cm depth) and one subsurface soil (10-20 cm depth). Comprehensive data on the sampling of these sediment and soil samples is provided in Table S1 in the supplementary material section.

Accuracy verification of the applied method. Due to the lack of certified reference samples in ^{135}Cs, the validity of the results on the collected soils and sediments was ensured by analyzing, two types of materials. The first was IAEA-330 and IAEA-375 certified reference materials (CRM) from the International Atomic Energy Agency (IAEA). Both CRMs were selected because of their frequent use in the validation of $^{135}Cs/^{137}Cs$ analysis protocols[1,12,32,36,37,44]. These samples of spinach (IAEA-330) and soil (IAEA-375) were respectively collected in Ukraine and Russia in 1990 and they show a $^{135}Cs/^{137}Cs$ ratio characteristic of Chernobyl fallout. In addition, three sediment samples exposed to high levels of Fukushima fallout were used. These sediment samples were collected in 2012, 2015 and 2020 in the Niida River catchment, which drains a part of the main radioactive plume in the

Fukushima Prefecture, Northeastern Japan[48]. Validity of the analytical method was evaluated by comparing the $^{135}Cs/^{137}Cs$ ratios measured in the IAEA and Niida samples with the published $^{135}Cs/^{137}Cs$ isotopic signature for the Chernobyl and Fukushima accidents, respectively [1,12,20,32,33,36–38].

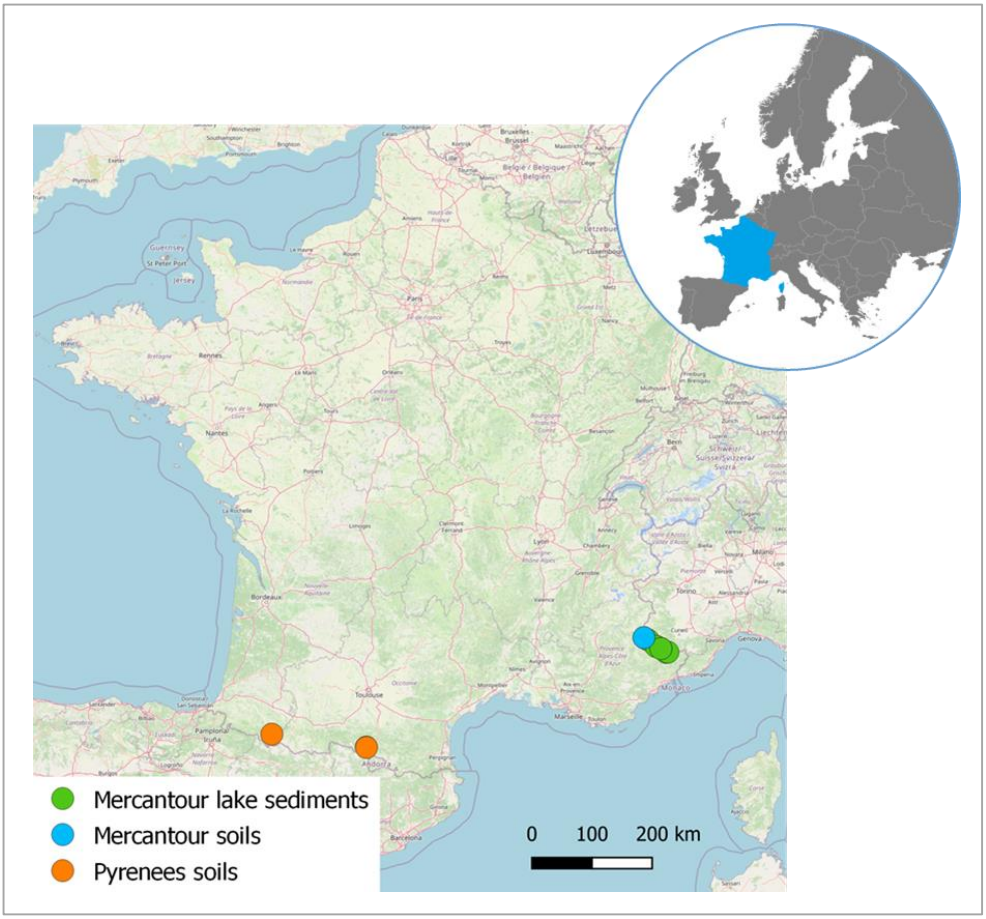

Figure 1: Location of sampling sites in France

Estimated contribution from each source of ^{137}Cs

Using bi-elemental isotopic signature: $^{239+240}Pu/^{137}Cs$. Nuclear Weapons Tests is considered the only source of airborne Pu in France[49,50]. Indeed after 1st may 1986, the contaminated air masses following Chernobyl accident contained mostly volatile fission products with negligible activity of plutonium[51]. Thus in the current work, assuming transuranics solely derived from NWT, we have used $^{239+240}Pu/^{137}Cs$ previously derived for NWT[25], for which an activity $^{239+240}Pu/^{137}Cs$ ratio of 0.04 ± 0.01 was found (decay-corrected to January 1st, 2022)[25] and the $^{239+340}Pu$ activity concentration ($Bq.kg^{-1}$) of the samples (namely $^{239+340}Pu_{samp}$) to deduced the ^{137}Cs from NWT in the samples (hereafter denoted as $^{137}Cs_{NWT}$) following (Eq. 1).

$$^{137}Cs_{\ NWT} = \frac{^{239+240}Pu_{samp}}{(^{239+240}Pu/^{137}Cs)_{REF}} \quad (1)$$

In this study, the activity of $^{239+240}Pu_{samp}$ was deduced from the gamma-ray or alpha spectrometry measurement of ^{241}Am (regarding $^{241}Am_{mes}$ refer to next section) and the $(^{241}Am/^{239+240}Pu)_{REF}$ activity ratio characteristic of the NWT, reported in the literature ($(^{241}Am/^{239+240}Pu)_{REF}$ = 0.39 ± 0.06, decay-corrected to January 1st, 2022)[23,26,52] (Eq. 2).

$$^{239+240}Pu_{\ samp} = \frac{^{241}Am_{mes}}{(^{241}Am/^{239+240}Pu)_{REF}} \quad (2)$$

Once the ^{137}Cs activity of NWT was calculated following equation (1), the proportion of ^{137}Cs resulting from the Chernobyl accident was deduced using the total ^{137}Cs activity measured by gamma-ray spectrometry (see next section).

Using a mono-elemental isotopic signature: $^{135}Cs/^{137}Cs$. Using mixing equation proposed by Bouisset et al. (2021)[53], the $^{135}Cs/^{137}Cs$ atomic ratios measured by mass spectrometry (ICP-MS/MS) in samples contaminated by two different sources (Chernobyl accident and NWT) is given by equation (3).

$$(^{135}Cs/^{137}Cs)_{measured} = x_{Chern}(^{135}Cs/^{137}Cs)_{Chern} + (1 - x_{Chern})(^{135}Cs/^{137}Cs)_{NWT} \quad (3)$$

where x_{Chern} and $(1 - x_{Chern})$ were the ^{137}Cs contributions from Chernobyl and NWT fallout, respectively. The $(^{135}Cs/^{137}Cs)_{Chern}$ and $(^{135}Cs/^{137}Cs)_{NWT}$ atomic ratios corresponded to the characteristic atomic ratios of both sources reported in the literature: 0.66 ± 0.03 and 3.70 ± 0.68 (decay-corrected to January 1st, 2022). It should be noted that the $^{135}Cs/^{137}Cs$ characteristic ratio of NWT reported was a "simple" average ratio considering the number of years since the period of testing (1950s to 1980s), assuming a $^{135}Cs/^{137}Cs$ atomic ratio of 1 at the date of each detonation[32,35]. The associated uncertainty was therefore significant compared, for example, to that of Chernobyl accident, which occurred at a specific date.

For each analyzed sample, the proportion of ^{137}Cs resulting from the Chernobyl accident (x_{Chern}) was estimated from equation (3) using a simple two end-member un-mixing model (Eq. 4).

$$x_{Chern} = \frac{(^{135}Cs/^{137}Cs)_{measured} - (^{135}Cs/^{137}Cs)_{NWT}}{(^{135}Cs/^{137}Cs)_{Chern} - (^{135}Cs/^{137}Cs)_{NWT}} \quad (4)$$

Methods applied to determine ^{137}Cs and ^{241}Am activities

Gamma-ray spectrometry measurements. Once collected, the soil and sediment samples were dried, crushed, sieved (< 2 mm) and then calcined at 500°C overnight in a muffle oven. The resulting ash was packed into a 60 mL Petri box ($Ø_{int}$=71 mm; h_{int}=15 mm) and measured by gamma-ray spectrometry. This first measurement aimed to assess the initial ^{137}Cs activity to determine the amount of sample to be analyzed to quantify the $^{135}Cs/^{137}Cs$ isotopic ratio and evaluate the chemical recoveries. The ^{241}Am activity was also measured by gamma-ray spectrometry.

The two gamma detectors employed were High-Purity Germanium (HPGe) distributed by Ortec with a crystal volume about 180 cm^3. For the first detector, the relative detection efficiency and resolution on the peak corresponding to ^{60}Co at 1332 keV were respectively 53% and 1.7 keV (IRSN/LMRE). The corresponding values amounted to 48% and 1.9 keV for the second detector (LSCE). The HPGe were previously calibrated in energy, resolution, and detection efficiency on the 40-1700 keV energy range using certified multigamma sources prepared by IRSN (IRSN/LEI, France). The activities of ^{137}Cs and ^{241}Am were respectively quantified using their characteristic emissions at 661.6 keV and 59.5 keV with long counting times (up to 24h) to improve the measurement statistics. The spectra analysis was performed with the GENIE 2000 software operated by Mirion Tech. Inc. and the "home-made" MadOni software. Then, corrections were applied to consider the self-attenuation effect according to the density and the matrix of the analyzed sample, and the used geometry.

In five of the samples in which ^{137}Cs contents exceeded $2x10^4$ $Bq.kg^{-1}$, the ^{241}Am activity could not be quantified by gamma-ray spectrometry due to the very high Compton effect caused by the significant presence of ^{137}Cs making difficult the discrimination of the peaks at low energy. In these samples, the ^{241}Am activity was measured by alpha spectrometry according to the analytical procedure described by Goutelard et al. (1998)[54] (see below) and used routinely in the laboratory (IRSN/LMRE) under COFRAC accreditation.

Alpha spectrometry for ^{241}Am activity measurements. For each sample, 1 to 2 grams of ash were introduced into a beaker and spiked with ^{243}Am to determine the chemical yield and the ^{241}Am activity. The samples were then leached at 150°C during 24h with concentrated HNO_3 and HCl in presence of hydrogen peroxide (H_2O_2). The solid residue was separated from the supernatant by centrifugation, leached again for 2h at 150°C with concentrated HNO_3 and rinsed with ultrapure water. The supernatants and rinse were combined. 15 g of oxalic acid were added to the solution with 5 mL of $CaCl_2$ at 100 $mg.g^{-1}$ and the mixture was adjusted to pH 1.5 to form a calcium oxalate

precipitate. After centrifugation, the precipitate was dried and destroyed by heating with 10 mL of concentrated HNO_3 and 5 mL of H_2O_2. The mixture was evaporated to dryness and the residue was dissolved in 40 mL of 8M HNO_3 with 0.2 g of $NaNO_2$. The americium was then purified using a series of four ion exchange resins. In detail, Am was separated from Pu(IV) using 6.4 g of AG®1-X8 resin (100 – 200 mesh, Cl^- form, Biorad Tech.) conditioned with 30 mL of 8M HNO_3. The sample was loaded and then the resin rinsed with 40 mL of 8M HNO_3. The sample eluate and rinses were combined, evaporated to dryness and the residue was dissolved in 10 mL of 9M HCl. Am was separated from Fe and U using a double column containing 6.5 g of AG®1-X8 resin and 2 g of AG®50W-X8 resin (100 – 200 mesh, H^+ form, Biorad Tech.). The sample loading and rinsing fractions (45 mL of 9M HCl) were again combined and evaporated. The residue was dissolved in 10 mL of 2M HNO_3/0.5M $Al(NO_3)_3$. The solution was purified of metals (Cu, Ni) with 0.7 g of TRU resin (100-150 µm, Triskem Int.). Once the sample was loaded and the resin rinsed (10 mL of 2M HNO_3), Am was eluted with 25 mL of 0.03M HNO_3. The eluate was evaporated to dryness and then redissolved in 20 mL of 1M HNO_3/93% CH_3OH mixture. Finally, Am was separated from Rare Earth Elements using 4 g of AG®1-X4 resin (100 – 200 mesh, Cl^- form, Biorad Tech.). The sample was loaded onto the resin and rinsed successively with 15 mL of 1M HNO_3/93% CH_3OH, 80 mL of 0.1M HCl/0.5M NH_4SCN/80% CH_3OH and 22 mL of 1M HNO_3/93%. Am was eluted from the AG®1-X4 resin with 75 mL of 1.5M HCl/86% CH_3OH mixture. The eluate was evaporated and dissolved was concentrated HNO_3, ultrapure H_2O and Na_2SO_4. The solution was adjusted to pH 1.90–1.95 and Am was electroplated for 2h at 1A on a stainless-steel disk. The disk was counted for 5 days using a low-level background α-spectrometer Alpha-Analyst (Canberra). The activity of ^{241}Am were quantified using its emitted-alpha particles at 5,485 keV.

It should be noted that all activities presented in this work were given with an uncertainty at k=2. For the ^{137}Cs and ^{241}Am measured activities, this uncertainty considered those related to counting statistics and detector calibration. Regarding the uncertainties of the $^{137}Cs_{NWT}$ and $^{239+240}Pu$ activities deduced by equation 1 and 2, they included the ^{241}Am measurement uncertainty and those associated with the $^{239+240}Pu/^{137}Cs$ and $^{241}Am/^{239+240}Pu$ reference ratios.

Method applied for $^{135}Cs/^{137}Cs$ isotopic ratio determination

Cs extraction and purification from solid matrices. The procedure of Cs extraction and purification from the environmental matrix was based on the analytical method described in our previous work[43]. 1 to 100 g of sample ash (depending on the measured ^{137}Cs activity) were introduced into a beaker. The radiocesium was extracted from the solid matrix by a succession of four acid leaching

steps of 8 hours on a hot plate with temperature set at 180°C. The first leaching was performed with 69.5% HNO_3 in presence of 30% H_2O_2 provided by Carlo Erba. The following leaching were carried out with a 69.5% HNO_3/37.5% HCl mixture (1:2, v/v) still in the presence of H_2O_2. Between successive leaching steps, the solid residue was separated from the supernatant by centrifugation. The supernatants were combined, evaporated to near dryness. The pH of the solution was adjusted to pH 1 – 2 by diluting the residue with ultrapure H_2O milli-Q H_2O (with resistivity 18.2 $M\Omega.cm^{-1}$) produced by a Merck Millipore system. 120 mg of ammonium molybdophosphate (AMP) powder (purchased from Alfa Aesar) were added to the solution to selectively complex Cs. The solution was then stirred for 30 minutes at room temperature and centrifuged for 15 minutes at 3500 rpm. After centrifugation, the supernatant was removed and the yellow precipitate containing Cs was filtered on a polyvinylidene fluoride membrane filter (PVDF, 0.45 µm pore size, Merck Millipore). The precipitate was washed with 5 mL of milli-Q H_2O and dissolved with 24 mL of 2M NH_4OH resulting in the complete decomposition of the AMP molecule and consequently, the release of Cs. Cs was then purified of all its interferents by combining the chemical properties of two extraction resins provided by Biorad Technologies. First, 3 mL of AG®MP-1M anion exchange resin (100 – 200 mesh, Cl^- form) conditioned with 1.5M NH_4OH were used to separate Cs from polyatomic interferents such as Mo, Sb and Sn. Under these conditions, Cs^+ ions were not adsorbed on the resin and were collected in the loading and rinsing fractions (2 x 3 mL of 1.5M NH_4OH), whereas Mo, Sb and Sn, present in oxide form, remained on it. Finally, Cs was separated from its isobaric interferent (Ba) using 8 mL of AG®50W-X8 cationic resin (100 – 200 mesh, H^+ form) conditioned with 20 mL of milli-Q H_2O followed by 20 mL of 1.5M NH_4OH. After the loading of the sample, the resin was rinsed with 50 mL of 1.5M NH_4OH and converted by 20 mL of milli-Q water followed by 20 mL of ultra-pure 1.5M HNO_3. Cs was selectively eluted with 50 mL of ultra-pure 1.5M HNO_3 while Ba remained fixed on the AG®50W-X8 resin. The eluate was measured by gamma-ray spectrometry, to estimate the chemical yield by monitoring ^{137}Cs. Then, it was evaporated to dryness and dissolved in 5 mL of ultrapure 0.5M HNO_3 to be measured by mass spectrometry.

ICP-MS/MS for $^{135}Cs/^{137}Cs$ isotopic ratio and interferent concentration measurements. Isotopic ratio and interferent content measurements were performed with the Agilent 8900#100 triple-quadrupole ICP-MS coupled with the SPS4 auto-sampler and controlled by the MassHunter 4.6 software. The formed ions in the hot plasma were extracted and focused with a Ni skimmer cone and a x-lens block. The instrument is equipped with an octupole reaction-collision cell (CRC) between two quadrupole mass filters (Q1 and Q2) allowing an efficient removal of interferences. All

measured solutions (blanks, standards, and samples) were prepared in 0.5M ultra-pure nitric acid and introduced into the ICP-MS by a MicroMist nebulizer with a peristaltic pump at 0.35 $mL.min^{-1}$ flow rate. The sensitivity and oxide rate settings were optimized using a multi-element solution concentrated to 2.5 $ng.g^{-1}$ in Cs, Ce and Ba prepared from certified solutions (Carlo Erba). Each measurement was corrected with an acid blank. All the experimental conditions are listed in Table S2.

The interferent (Ba, Mo, Sb, Sn) contents were monitored in single quadrupole mode without reaction gas and calculated by an external calibration method. The standards were prepared from ultra-pure milli-Q water and certified mono-elemental solutions provided by Carlo Erba. The matrix effect was corrected using indium as internal standard (concentrated to 3 $ng.g^{-1}$).

The $^{135}Cs/^{137}Cs$ isotopic ratios were quantified in triple quadrupole mode by setting Q1 and Q2 to the 135 and 137 m/z. To effectively remove the last traces of interferences, a mixture of N_2O (99.998% purity, Messer), He (99.9992% purity, Air product) and NH_3/He (10/90 m/m, 99.98% purity, Air product) was added in the CRC with flow rates of about 0.55, 1 and 4.79 $mL.min^{-1}$, respectively. Isotopic ratios were corrected for mass bias by the sample standard bracketing approach with a solution with a known $^{135}Cs/^{137}Cs$ ratio delivered by DES-SEARS (CEA). The uncertainty associated with the corrected ratio were also given at k=2. It considered the variation of the ICP-MS/MS signal during the measurement of the sample and the uncertainty of the mass bias correction.

Evaluation of the chemical performance. The chemical performances (recovery yield and eluate purity) achieved for each sample are detailed in Table S3. Recovery yields were estimated by monitoring ^{137}Cs by gamma-ray spectrometry in both the solid and purified liquid samples. They ranged from 57% to 93%. Regarding potential spectral interferences during the analyses, the radiochemical treatment of the samples allowed to significantly reduce the levels of Ba, Mo, Sb and Sn in the measurement fraction, with contents ranging from 0.1 to 5.4, 0.13 to 17.5, 0.03 to 0.46, and 0.2 to 12.2 $ng.g^{-1}$, respectively. To accurately measure the $^{135}Cs/^{137}Cs$ ratio, these traces of interferents that remained present in solution were effectively removed by adding a mixture of reaction gases (N_2O, NH_3, He) in the CRC of the mass spectrometer.

Results and Discussion

Tracing the origin of radiocesium contamination by measuring ^{137}Cs and ^{241}Am activities by nuclear counting – Use of bi-elemental isotopic signatures.

The activities of ^{137}Cs and ^{241}Am in lake sediment, surface soil and subsurface soil samples collected in France are presented in Table 1. Regarding ^{137}Cs, a significant heterogeneity of activities was found between the two main sampling regions (Mercantour Massif or the Pyrenees) as well as, within the same region, between the analyzed matrices (sediment or soil). The highest variability was obtained in the Mercantour soils (including surface and subsurface soils) with values ranging from a few tens (165 ± 11) to several tens of thousands (103,308 ± 113) of $Bq.kg^{-1}$. Such a strong heterogeneity is consistent with "enrichment spots", *i.e.* surfaces of a few dm^2 strongly concentrating ^{137}Cs from Chernobyl fallout[46]. In contrast, ^{137}Cs activities measured in the soils of the Pyrenees exhibited low heterogeneity and were about 2 to 7 times lower than in the Mercantour, with levels ranging between 23 ± 4 and 93 ± 28 $Bq.kg^{-1}$. An explanation to this lower heterogeneity is that the nuclear weapon tests occurred over a longer period (between the 1950s and 1980s). Overall, for both regions, ^{137}Cs activity decreased with increasing sampling depths. For the sediments from the Mercantour lakes, the ^{137}Cs concentrations were significant and relatively homogeneous compared to the soils, with activities varying from 249 ± 19 to 5,274 ± 350 $Bq.kg^{-1}$. For each site and each matrix studied, the distribution of ^{137}Cs activities was in good agreement with that reported in the literature[21,46,47]. High to very high levels of ^{137}Cs were expected in the Mercantour resulting from a superposition of deposition from NWT and the Chernobyl accident. In contrast, the Pyrenees soils showed lower activities, which was expected as they were hypothesized to have been mainly supplied by the NWT. These preliminary interpretations were confirmed with the assessment of the ^{137}Cs contributions of each source using the $^{241}Am/^{239+240}Pu$ and then the $^{239+240}Pu/^{137}Cs$ ratios provided for the NWT (see experimental section) (Table 1). They show, overall, that the proportion of ^{137}Cs from Chernobyl fallout increases significantly with the total ^{137}Cs activity while the ^{137}Cs activity resulting from the NWT remains relatively homogenous (28 to 606 $Bq.kg^{-1}$) for both studied mountainous areas and both environmental matrix (cf. Figure 2). Thus, the use of bi-elemental signatures ($^{241}Am/^{239+240}Pu$ and $^{239+240}Pu/^{137}Cs$) allowed, in a first step, to estimate the contributions of each ^{137}Cs source. Nevertheless, the hypothesis of the fractionation of two elements with different bio-geochemical properties (*i.e.,* Am vs. Pu, Pu vs. Cs) cannot be fully excluded, although they were described in the literature to be relatively similar[55,56].

325

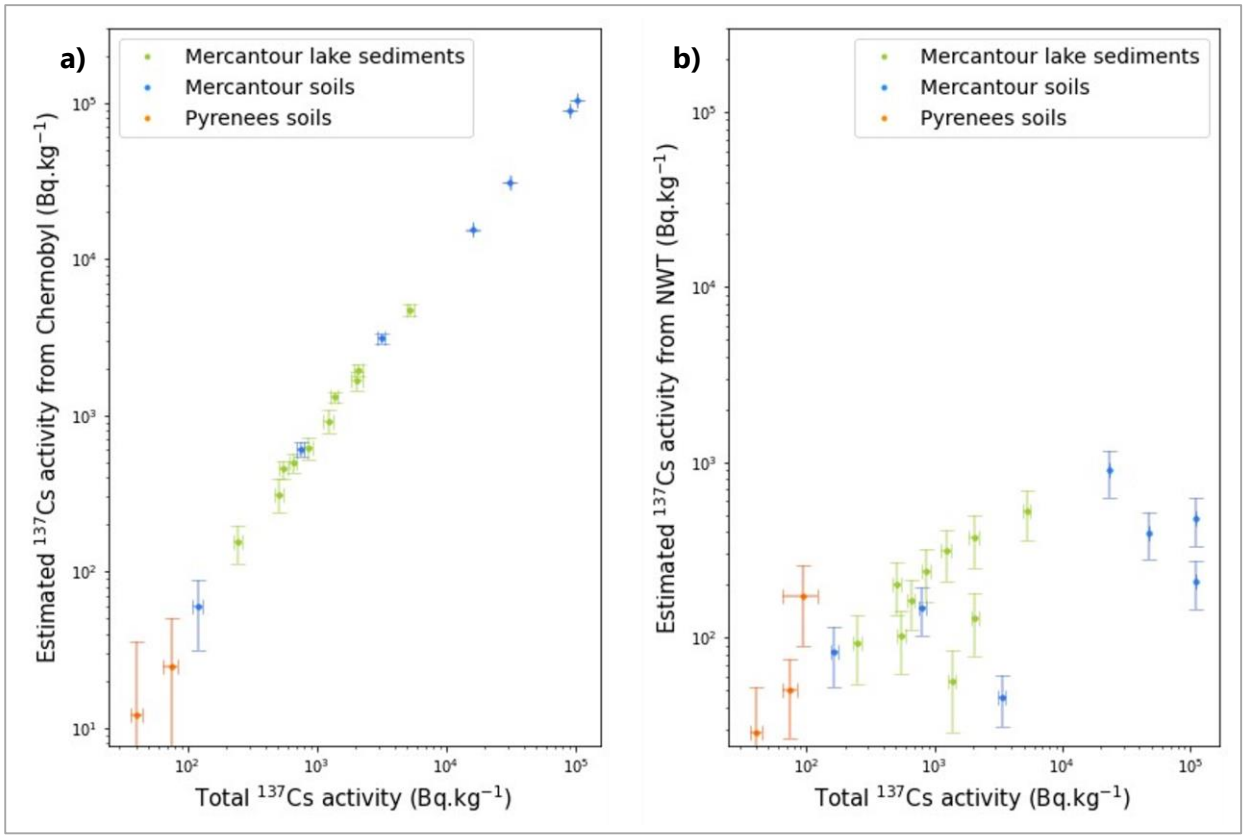

Figure 2: Distribution of the estimated ^{137}Cs activity resulting from the Chernobyl accident (a) and nuclear weapons testing (b) as a function of total ^{137}Cs activity measured by gamma-ray spectrometry in soil and sediment samples collected in France. All activities are decay-corrected to January 1, 2022, and the error bars correspond to a measurement uncertainty at k = 2. ^{137}Cs/$^{239+240}$Pu is used here to estimate the respective sources of ^{137}Cs. (see experimental section)

Table 1: ^{137}Cs and ^{241}Am activities measured by gamma-ray spectrometry in sediments and soils of the investigated sites as decay-corrected to January 1st, 2022, and with uncertainty at k=2. $^{239+240}Pu$, ^{137}Cs activities resulting from nuclear weapons testing (NWT) and ^{137}Cs from Chernobyl (Chern) deduced from $^{241}Am/^{239+240}Pu$ and $^{239+240}Pu/^{137}Cs$ activity ratios reported in the literature for NWT contribution (0.40 ± 0.06 and 0.04 ± 0.01 respectively, and decay-corrected to January 1st, 2022) (see experimental section).

Sample name	Matrix	Study area	Sampling site	Depth (cm)	^{137}Cs activity (Bq.kg^{-1} dry)	^{241}Am activity (Bq.kg^{-1} dry)	$^{239+240}Pu_{NWT}$ activity (Bq.kg^{-1})	$^{137}Cs_{NWT}$ activity (Bq.kg^{-1})	$^{137}Cs_{Chern}$ activity (Bq.kg^{-1})
20_PNM45_1	Lake sediment	Mercantour mountain	Main Terre Rouge lake	—	1234 ± 114	4.99 ± 0.71	12.48 ± 2.59	312 ± 101	922 ± 159
20_PNM45_2			Temporary Terre rouge lake	—	2047 ± 193	5.98 ± 0.97	14.95 ± 3.30	374 ± 125	1673 ± 259
20_PNM45_3			Superior Lausfer lake	—	513 ± 38	3.21 ± 0.48	8.02 ± 1.70	200 ± 66	313 ± 76
20_PNM45_4			Inferior Lausfer lake	—	249 ± 19	1.50 ± 0.46	3.75 ± 1.27	94 ± 39	155 ± 44
13-PNM4			Cerise lake	—	1375 ± 95	0.90 ± 0.36	2.25 ± 0.96	56 ± 28	1319 ± 99
13-PNM7			Besson lake	—	2086 ± 155	2.05 ± 0.54	5.11 ± 1.56	128 ± 50	1958 ± 163
13-PNM9			Vens lake	—	555 ± 40	1.63±0.42	4.08 ± 1.22	102 ± 40	453 ± 57
13-PNM19			Lausfer lake	—	862 ± 66	3.82 ± 0.57	9.54 ± 2.02	239 ± 78	624 ± 102
21_PNM24_5			Terre Rouge Main lake	—	659 ± 45	2.58 ± 0.33	6.46 ± 1.27	161 ± 51	497 ± 68
21_PNM24_6			Terre Rouge Inferior lake	—	5274 ± 350	8.43 ± 0.99	21.07 ± 4.01	527 ± 166	4747 ± 387
21_PNM24_1	Soil	Mercantour mountain	Restefond pass	0 – 5	89,894 ± 90	6.15 ± 0.54*	15.37 ± 2.68	384 ± 117	89,510 ± 148
				5 – 10	103,501 ± 97	3.08 ± 0.31*	7.70 ± 1.39	192 ± 59	103,308 ± 113
21_PNM24_2				0 – 5	165 ± 11	1.34 ± 0.32	3.34 ± 0.95	84 ± 32	82 ± 34
21_PNM24_3				0 – 5	31,214 ± 96	4.16 ± 0.49*	10.40 ± 1.99	260 ± 82	30,954 ± 126
				5 – 10	3169 ± 223	0.68 ± 0.10*	1.69 ± 0.36	45 ± 15	3321 ± 224
21_PNM24_4				0 – 5	16,066 ± 32	9.69 ± 0.94*	24.23 ± 4.32	606 ± 186	15,460 ± 189
				5 – 10	803 ± 53	2.38 ± 0.25	5.95 ± 1.09	149 ± 46	654 ± 70
14_PYR_2		Pyrenees	Coumebière plateau	0 – 10	75 ± 10	0.81 ± 0.31	2.02 ± 0.82	51 ± 24	25 ± 26
14_PYR_3			Labant pond	0 – 10	93 ± 28	2.78 ± 1.08	6.95 ± 2.90	174 ± 84	*< 1,03*
				10 – 20	23 ± 4	*< 0.36*	—	—	—
14_PYR_53			Besse pass	0 – 10	40 ± 4	0.46 ± 0.35	1.14 ± 0.88	28 ± 23	12 ± 24

** Alpha spectrometry measurement*

Tracing the origin of radiocesium contamination using the $^{135}Cs/^{137}Cs$ isotopic ratio measured by ICP-MS/MS – Use of mono-elemental isotopic signature.

The analytical procedure to quantify the $^{135}Cs/^{137}Cs$ isotopic ratio in environmental samples was first applied to samples known to be contaminated with Chernobyl (IAEA-330 and IAEA-375)[1,20,32,36,37] or Fukushima fallout (Niida_2012, Niida_2015 and Niida_2020)[48]. The analytical results are presented in Table 2 and they were compared with the few data available in the literature for both sources of accidental contamination. To facilitate the comparison of results, all isotopic ratios were decay-corrected to January 1st, 2022. For both IAEA reference samples, which are generally used in the literature to validate the $^{135}Cs/^{137}Cs$ ratio analysis methods, the measured ratios (0.66 ± 0.06 and 0.67 ± 0.02) agreed well with those reported in the literature[1,20,32,36,37] (ranging from 0.66 ± 0.06 to 0.68 ± 0.13). In the absence of certified reference materials characteristic of Fukushima fallout, the $^{135}Cs/^{137}Cs$ isotopic ratios obtained in the sediments collected in the Niida river catchment were compared with the ratios published by studies characterizing the Fukushima fallout. For these sediments, the average measured $^{135}Cs/^{137}Cs$ ratios of 0.47 ± 0.02 was fully consistent with the ratios reported in the literature[12,33,36,38] and ranging from 0.45 ± 0.03 to 0.47 ± 0.04. This comparison demonstrated the reliability of the analytical procedure.

Table 2: $^{135}Cs/^{137}Cs$ isotopic ratios measured by ICP-MS/MS for materials impacted by Chernobyl (IAEA-330 and IAEA-375) and Fukushima (Niida_2012, Niida_2015 and Niida_2020) fallout. Comparison of these ratios with isotopic signatures reported in the literature for these contamination sources.

Sample name	**Main source of ^{137}Cs**	**$^{135}Cs/^{137}Cs$ isotopic ratio** *(at/at)*		
		Current work	**Literature values**	
IAEA-330	Chernobyl fallout	0.66 ± 0.06 (n=3)	0.66 ± 0.06	*Taylor et al. (2008)*
			0.66 ± 0.03	*Zheng et al. (2014)*
			0.66 ± 0.06	*Snow et al. (2015)*
			0.66 ± 0.13	*Zhu et al. (2020)*
IAEA-375		0.67 ± 0.02 (n=3)	0.68 ± 0.10	*Zheng et al. (2014)*
			0.66 ± 0.03	*Snow et al. (2015)*
			0.68 ± 0.03	*Dunne et al. (2017)*
			0.68 ± 0.13	*Zhu et al. (2020)*
Niida_2012	Fukushima fallout	0.47 ± 0.02 (n=3)	0.47 ± 0.04	*Ohno et al. (2014)*
Niida_2015		0.46 ± 0.01 (n=3)	0.45 ± 0.03	*Zheng et al. (2014)*
			0.45 ± 0.02	*Yang et al. (2016)*
Niida_2020		0.49 ± 0.04 (n=1)	0.46 ± 0.01	*Zok et al. (2021)*

Decay-corrected to January 1st, 2022. The isotopic ratios are provided with uncertainty at k = 2.

349 Once the analytical procedure to measure $^{135}Cs/^{137}Cs$ was validated, it was applied to lake sediment
350 and soil samples collected in France (Table 3).

351 *Table 3: $^{135}Cs/^{137}Cs$ isotopic ratios in lake sediments and soils collected in France.*

Sample name	Matrix	Study area	Sampling site	Depth *(cm)*	^{137}Cs activity *($Bq.kg^{-1}$)*	$^{135}Cs/^{137}Cs$ atomic ratio *(at/at)*	Proportion of ^{137}Cs from Chernobyl accident
20_PNM45_1	Lake sediment	Mercantour mountain	Main Terre Rouge lake	—	1234 ± 114	1.64 ± 0.05	68%
20_PNM45_2			Temporary Terre Rouge lake	—	2047 ± 193	1.23 ± 0.10	81%
20_PNM45_3			Superior Lausfer lake	—	513 ± 38	2.29 ± 0.05	46%
20_PNM45_4			Inferior Lausfer lake	—	249 ± 19	2.18 ± 0.24	50%
13-PNM4			Cerise lake	—	1375 ± 95	0.85 ± 0.08	94%
13-PNM7			Besson lake	—	2086 ± 155	1.06 ± 0.09	87%
13-PNM9			Vens lake	—	555 ± 40	1.41 ± 1.86	75%
13-PNM19			Lausfer lake	—	862 ± 66	1.86 ± 0.13	61%
21_PNM24_5			Terre Rouge Main lake	—	659 ± 45	1.46 ± 0.22	74%
21_PNM24_6			Terre Rouge Inferior lake	—	5274 ± 350	1.07 ± 0.03	87%
21_PNM24_1	Soil	Mercantour mountain	Restefond pass	0 – 5	89,894 ± 90	0.68 ± 0.01	99%
				5 – 10	103,501 ± 97	0.66 ± 0.04	100%
21_PNM24_2				0 – 5	165 ± 11	2.27 ± 0.29	47%
21_PNM24_3				0 – 5	31,214 ± 96	0.71 ± 0.02	98%
				5 – 10	3169 ± 223	0.71 ± 0.03	98%
21_PNM24_4				0 – 5	16,066 ± 32	0.75 ± 0.02	97%
				5 – 10	803 ± 53	1.00 ± 0.07	89%
14_PYR_2		Pyrenees	Coumebière plateau	0 – 10	75 ± 10	4.29 ± 0.21	*-19%*
14_PYR_3			Labant pond	0 – 10	93 ± 28	4.26 ± 0.66	*-18%*
				10 – 20	23 ± 4	3.94 ± 0.89	*-8%*
14_PYR_53			Besse pass	0 – 10	40 ± 4	4.04 ± 0.75	*-11%*

Data are decay-corrected to January 1st, 2022. All results presented are provided with an uncertainty at k = 2.

352

The analytical results show strongly variable $^{135}Cs/^{137}Cs$ signatures with a minimum value of 0.66 ± 0.04 in a Mercantour soil and a maximum value of 4.29 ± 0.21 in a soil sample from the Pyrenees. It is noteworthy that soils from this area show nearly homogenous isotopic ratios, ranging from 3.94 ± 0.89 to 4.29 ± 0.21. Compared with the isotopic signatures reported for each source in the literature or in Table 2 of the current research (NWT, Chernobyl, and Fukushima accidents), such a low $^{135}Cs/^{137}Cs$ was consistent with the Chernobyl fallout signature, while the highest ratio lied within the range of values attributed to the NWT (Figure 3).

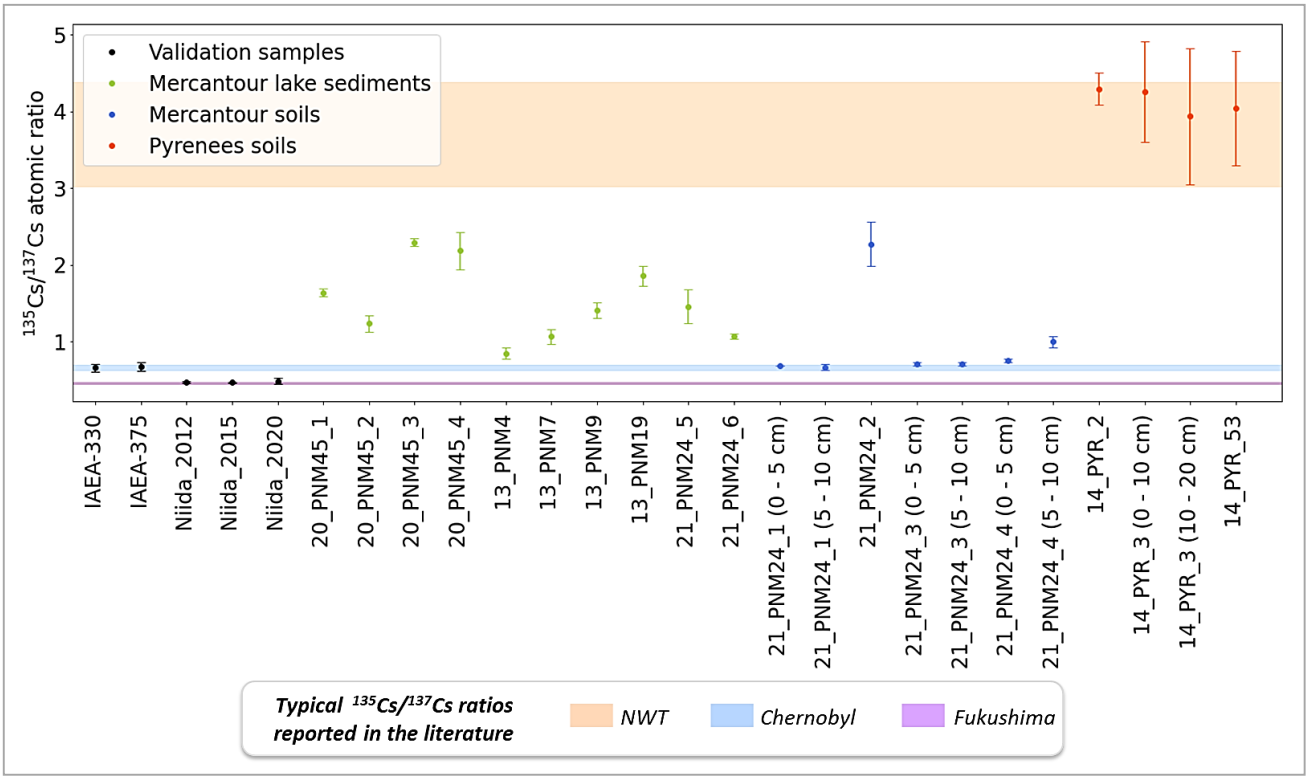

Accordingly, it can be deduced that the ^{137}Cs radioactive contamination of the 21_PNM24_1

Figure 3: $^{135}Cs/^{137}Cs$ atomic ratios measured by ICP-MS/MS (decay-corrected to January 1st, 2022) in the samples used for method validation (IAEA and Niida) and in French soils and sediments collected in the two investigated areas. The error bars correspond to a measurement uncertainty at k = 2 and the colored bands represent the typical $^{135}Cs/^{137}Cs$ ratios of the three main fallout sources.

Mercantour soil was almost exclusively due to the Chernobyl accident fallout while that of the Pyrenees soils was almost exclusively due to the fallout of nuclear weapons testing. Nevertheless, it should be noted that the ^{137}Cs contributions of Chernobyl fallout calculated for soil samples from the Pyrenees (Table 3) were slightly negative, due to the uncertainty of NWT signature, with, as underlined in the introduction, only two values of $^{135}Cs/^{137}Cs$ available for this source in the literature up to now[32,35]. This could be also explained by the fact that these estimates relied on a $^{135}Cs/^{137}Cs$ ratio value characteristic of NWT averaged over the entire testing period (1950s to 1980s) assuming a $^{135}Cs/^{137}Cs$ ratio of 1 at the date of detonation[35]. However, the value of this ratio

could be refined based on the proportion of ^{137}Cs deposited during each year due to fallout from NWT, while still assuming a $^{135}Cs/^{137}Cs$ ratio of 1 at the time of testing. Considering the proportion of annual deposition of ^{137}Cs between 1958 and 1980 given by UNSCEAR[4] and assuming the accumulation of cesium with time in the soil or the sediments, the average $^{135}Cs/^{137}Cs$ ratio of the resulting deposit would be about 3.94 to the reference time of January 1st, 2022, close to the average value reported for NWT is 3.70[32,35] (Table S4). According to experimental $^{135}Cs/^{137}Cs$ ratios (3.94 ± 0.89 to 4.29 ± 0.21), actual deposition by NWT in the Pyrenees has likely mainly occurred in the early period of 1950s to 1980s. Nevertheless, due to the limited data on the impact of NWT fallout before the 1960s in the Pyrenees, it is difficult to determine an average value for the $^{135}Cs/^{137}Cs$ ratio, specific for this region. The main limitation of this method is therefore the uncertainty in the regional variation of ^{135}Cs and ^{137}Cs deposits due to nuclear weapons testing.The other Mercantour soil and sediments samples with $^{135}Cs/^{137}Cs$ ranging between 0.68 ± 0.01 and 2.29 ± 0.05 showed radioactive contamination constituted of a mix of both sources in variable proportions. Thus, for each sample, the proportion of ^{137}Cs resulting from Chernobyl fallout was estimated using simple un-mixing models following methodology given in experimental section (Table 3). In addition, the data highlighted a relationship between ^{137}Cs activity estimated by gamma-ray spectrometry and the $^{135}Cs/^{137}Cs$ isotopic ratio measured by ICP-MS/MS. As shown in Figure 4, when the ^{137}Cs activity increased, the $^{135}Cs/^{137}Cs$ ratio decreased until it reached the $^{135}Cs/^{137}Cs$ isotopic signature of Chernobyl fallout. Similarly, to the trend of $^{135}Cs/^{137}Cs$, a trend of $^{134}Cs/^{137}Cs$ variations in soils of the Mercantour mountain has been shown on the one hand soils strongly enriched in ^{137}Cs originating from Chernobyl and on the other hand other soils with low ^{137}Cs contamination due to NWT fallout[46]. Thus, both trends involving isotopes ratios of Cs suggest that soils and sediments contain the two sources (NWT and Chernobyl) in various proportions from one sample to another.

All these observations agree with what was previously predicted and, therefore, demonstrate the applicability of the $^{135}Cs/^{137}Cs$ ratio to discriminate unambiguously the sources of radioactive contamination. Moreover, the use of a mono-elemental isotopic signature such as $^{135}Cs/^{137}Cs$ ratio allows to get rid of any potential fractionation caused the potential difference of behavior between two elements (such as Am and Pu or Pu and Cs), even if they share very similar chemical properties.

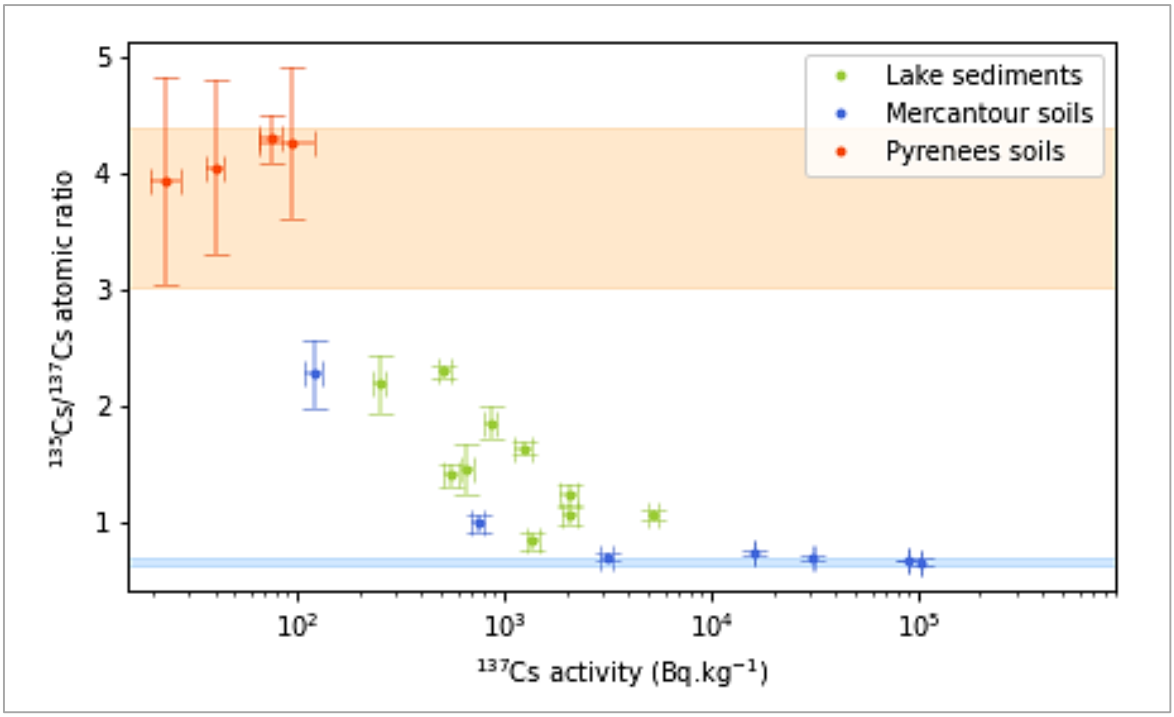

Figure 4: Relationship between $^{135}Cs/^{137}Cs$ isotopic ratios and ^{137}Cs activity in sediments and soils collected in the Mercantour massif and the Pyrenees, France. The dark blue and orange bands indicate the typical $^{135}Cs/^{137}Cs$ ratios reported in the literature for fallout from nuclear weapons testing (NWT) and the Chernobyl accident. All data were decay-corrected to January 1st, 2022.

Conclusions

The main objective of the current research was to improve our knowledge of the radiological background in environments remote from nuclear tests or nuclear accident sites by analysing an isotopic signature little exploited to date, i.e., the $^{135}Cs/^{137}Cs$ ratio. We have recently developed an analytical method to measure this ratio in solid environmental matrices and have applied it to soil and sediment samples collected in two areas of interest in France (Pyrenees and Mercantour massif). $^{135}Cs/^{137}Cs$ ratios ranging from 0.66 ± 0.04 in Mercantour soils to 4.29 ± 0.21 in Pyrenees soils were measured corresponding to typical ratios reported in the literature for Chernobyl accident fallout and from nuclear weapons tests, respectively. From these results, the contribution of each of these sources could be estimated and successfully compared with those calculated from more commonly used diagnostic ratios ($^{241}Am/^{239+240}Pu$ and $^{239+240}Pu/^{137}Cs$). Accordingly, the current work demonstrates the strength of the $^{135}Cs/^{137}Cs$ isotopic ratio as a novel fingerprint for identifying the radioactive contamination sources and estimating their contribution in the environment. Moreover, the monitoring of this isotopic ratio in the areas that were the most affected by the Chernobyl and Fukushima accidents could provide a surrogate for the $^{134}Cs/^{137}Cs$ ratio, as the use of this ratio is

limited in time given the rapid decay of ^{134}Cs. In future research, it could be interesting to consider the potential occurrence of diagnostic signatures of radiocesium released by nuclear facilities.

Acknowledgement

G. Salaün is warmly acknowledged for his excellent field work in the Alps and Pyrenees mountains and his expertise for preparation of the samples in the laboratory.

We thank S. Aubry and S. Bonnot from the gamma team of the LMRE for the measurements of ^{137}Cs and ^{241}Am by gamma-ray spectrometry and also S. Thomas for her recommendations on the ^{241}Am measurement by alpha spectrometry.

We also warmly thank H. Isnard and S. Mialle from the Laboratory of Analytical development for Nuclear Isotopic and Elemental analysis (CEA) for the supply and qualification of the spent fuel sample used in this research to correct the $^{135}Cs/^{137}Cs$ isotopic ratios during the ICP-MS/MS measurements.

References

(1) Snow, M. S.; Snyder, D. C.; Mann, N. R.; White, B. M. Method for Ultra-Trace Cesium Isotope Ratio Measurements from Environmental Samples Using Thermal Ionization Mass Spectrometry. *International Journal of Mass Spectrometry* **2015**, *381–382*, 17–24. https://doi.org/10.1016/j.ijms.2015.03.006.

(2) Steinhauser, G.; Brandl, A.; Johnson, T. E. Comparison of the Chernobyl and Fukushima Nuclear Accidents: A Review of the Environmental Impacts. *Science of The Total Environment* **2014**, *470–471*, 800–817. https://doi.org/10.1016/j.scitotenv.2013.10.029.

(3) *Tchernobyl 10 ans après*; Dossier de presse IPSN/96/10232/LP; IPSN, 1996; p 50.

(4) UNSCEAR. *Ionizing Radiation: Sources and Biological Effects*; New York, 1982.

(5) UNSCEAR. *Levels and effects of radiation exposure due to the accident at the Fukushima Daiichi nuclear power station: implications of information published since the UNSCEAR 2013 Report.*; 2021.

(6) Dunne, J. A.; Martin, P. G.; Yamashiki, Y.; Ang, I. X. Y.; Scott, T. B.; Richards, D. A. Spatial Pattern of Plutonium and Radiocaesium Contamination Released during the Fukushima Daiichi Nuclear Power Plant Disaster. *Sci Rep* **2018**, *8* (1), 16799. https://doi.org/10.1038/s41598-018-34302-0.

(7) Wan Mahmood, Z. U.; Yii, M. W.; Khalid, M. A.; Yusof, M. A. W.; Mohamed, N. Marine Radioactivity of Cs-134 and Cs-137 in the Malaysian Economic Exclusive Zone after the Fukushima Accident. *J Radioanal Nucl Chem* **2018**, *318* (3), 2165–2172. https://doi.org/10.1007/s10967-018-6306-2.

(8) Aoyama, M. Long-Range Transport of Radiocaesium Derived from Global Fallout and the Fukushima Accident in the Pacific Ocean since 1953 through 2017—Part I: Source Term and

Surface Transport. *J Radioanal Nucl Chem* **2018**, *318* (3), 1519–1542. https://doi.org/10.1007/s10967-018-6244-z.

(9) Brimo, K.; Gonze, M. A.; Pourcelot, L. Long Term Decrease of 137Cs Bioavailability in French Pastures: Results from 25 Years of Monitoring. *Journal of Environmental Radioactivity* **2019**, *208–209*, 106029. https://doi.org/10.1016/j.jenvrad.2019.106029.

(10) Chao, J.-H.; Tseng, C.-L. Determination of 135Cs by Neutron Activation Analysis. *Nuclear Instruments and Methods in Physics Research Section A: Accelerators, Spectrometers, Detectors and Associated Equipment* **1996**, *372* (1), 275–279. https://doi.org/10.1016/0168-9002(95)01296-6.

(11) Qiao, J.; Hansen, V.; Hou, X.; Aldahan, A.; Possnert, G. Speciation Analysis of 129I, 137Cs, 232Th, 238U, 239Pu and 240Pu in Environmental Soil and Sediment. *Applied Radiation and Isotopes* **2012**, *70* (8), 1698–1708. https://doi.org/10.1016/j.apradiso.2012.04.006.

(12) Zok, D.; Blenke, T.; Reinhard, S.; Sprott, S.; Kegler, F.; Syrbe, L.; Querfeld, R.; Takagai, Y.; Drozdov, V.; Chyzhevskyi, I.; Kirieiev, S.; Schmidt, B.; Adlassnig, W.; Wallner, G.; Dubchak, S.; Steinhauser, G. Determination of Characteristic vs Anomalous 135Cs/137Cs Isotopic Ratios in Radioactively Contaminated Environmental Samples. *Environ. Sci. Technol.* **2021**, *55* (8), 4984–4991. https://doi.org/10.1021/acs.est.1c00180.

(13) Bérard, P.; Le Guen, B.; Perrin, M. L.; Desprès, A.; Gaillard-Lecanu, E.; Chambrette, V.; Brenot, J. Fiche radionucléide - Cesium 137 + Baryum 137m, 2001.

(14) Gray, J.; Jones, S. R.; Smith, A. D. Discharges to the Environment from the Sellafield Site, 1951-1992. *J. Radiol. Prot.* **1995**, *15* (2), 99–131. https://doi.org/10.1088/0952-4746/15/2/001.

(15) Buesseler, K.; Aoyama, M.; Fukasawa, M. Impacts of the Fukushima Nuclear Power Plants on Marine Radioactivity. *Environ. Sci. Technol.* **2011**, *45* (23), 9931–9935. https://doi.org/10.1021/es202816c.

(16) Colle, C.; Adam, C.; Garnier-Laplace, J.; Roussel-Debet, S. Fiche Radionucléide - Césium 137 et Environnement, 2005.

(17) de Vismes Ott, A.; Gurriaran, R.; Cagnat, X.; Masson, O. Fission Product Activity Ratios Measured at Trace Level over France during the Fukushima Accident. *Journal of Environmental Radioactivity* **2013**, *125*, 6–16. https://doi.org/10.1016/j.jenvrad.2013.02.014.

(18) Zettwoog, P.; Lemaître, N.; Bernard, S.; Vauzelle, Y. Utilisation de La Signature Isotopique Des Radionucléides Relâchés Par Les Mines et Les Usines de Traitement de Minerais d'uranium Pour Discriminer Aux Bas Niveaux Leur Impact Environnemental de Celui de La Radioactivité Tellurique Naturelle. *Radioprotection* **1997**, *32* (4), 467–489. https://doi.org/10.1051/radiopro:1997114.

(19) Moreno, J. M. B.; Betti, M.; Nicolaou, G. Determination of Caesium and Its Isotopic Composition in Nuclear Samples Using Isotope Dilution-Ion Chromatography-Inductively Coupled Plasma Mass Spectrometry. *J. Anal. At. Spectrom.* **1999**, *14* (5), 875–879. https://doi.org/10.1039/A806467I.

(20) Taylor, V. F.; Evans, R. D.; Cornett, R. J. Preliminary Evaluation of (135)Cs/(137)Cs as a Forensic Tool for Identifying Source of Radioactive Contamination. *J Environ Radioact* **2008**, *99* (1), 109–118. https://doi.org/10.1016/j.jenvrad.2007.07.006.

(21) Meusburger, K.; Evrard, O.; Alewell, C.; Borrelli, P.; Cinelli, G.; Ketterer, M.; Mabit, L.; Panagos, P.; van Oost, K.; Ballabio, C. Plutonium Aided Reconstruction of Caesium Atmospheric Fallout in European Topsoils. *Sci Rep* **2020**, *10* (1), 11858. https://doi.org/10.1038/s41598-020-68736-2.

(22) Alewell, C.; Meusburger, K.; Juretzko, G.; Mabit, L.; Ketterer, M. E. Suitability of 239+240Pu and 137Cs as Tracers for Soil Erosion Assessment in Mountain Grasslands. *Chemosphere* **2014**, *103*, 274–280. https://doi.org/10.1016/j.chemosphere.2013.12.016.

(23) IRSN. *Constat Radiologique "Rémanence de la radioactivité d'origine artificielle";* PRP-ENV/SESURE 2015-41; IRSN, 2016; p 130. https://www.irsn.fr/FR/expertise/rapports_expertise/surveillance-environnement/Documents/IRSN_Constat-Remanence-France_201604.pdf.
(24) Cizdziel, J.; Hodge, V.; Faller, S. Resolving Nevada Test Site and Global Fallout Plutonium in Attic Dust and Soils Using 137Cs/239+240Pu Activity Ratios. *Health Phys* **1999**, *77* (1), 67–75. https://doi.org/10.1097/00004032-199907000-00012.
(25) Hodge, V.; Smith, C.; Whiting, J. Radiocesium and Plutonium: Still Together in "Background" Soils after More than Thirty Years. *Chemosphere* **1996**, *32* (10), 2067–2075. https://doi.org/10.1016/0045-6535(96)00108-7.
(26) Bunzl, K.; Kracke, W. Cumulative Deposition of 137Cs, 238Pu, 239+240Pu and 241Am from Global Fallout in Soils from Forest, Grassland and Arable Land in Bavaria (FRG). *Journal of Environmental Radioactivity* **1988**, *8* (1), 1–14. https://doi.org/10.1016/0265-931X(88)90010-0.
(27) Carbol, P.; Solatie, D.; Erdmann, N.; Nylén, T.; Betti, M. Deposition and Distribution of Chernobyl Fallout Fission Products and Actinides in a Russian Soil Profile. *Journal of Environmental Radioactivity* **2003**, *68* (1), 27–46. https://doi.org/10.1016/S0265-931X(03)00027-4.
(28) Chino, M.; Terada, H.; Nagai, H.; Katata, G.; Mikami, S.; Torii, T.; Saito, K.; Nishizawa, Y. Utilization of 134Cs/137Cs in the Environment to Identify the Reactor Units That Caused Atmospheric Releases during the Fukushima Daiichi Accident. *Sci Rep* **2016**, *6* (1), 31376. https://doi.org/10.1038/srep31376.
(29) Shibahara, Y.; Kubota, T.; Fujii, T.; Fukutani, S.; Ohta, T.; Takamiya, K.; Okumura, R.; Mizuno, S.; Yamana, H. Analysis of Cesium Isotope Compositions in Environmental Samples by Thermal Ionization Mass Spectrometry – 1. A Preliminary Study for Source Analysis of Radioactive Contamination in Fukushima Prefecture. *Journal of Nuclear Science and Technology* **2014**, *51* (5), 575–579. https://doi.org/10.1080/00223131.2014.891954.
(30) Thomas, A. J.; Martin, J. M. First Assessment of Chernobyl Radioactive Plume over Paris. *Nature* **1986**, *321* (6073), 817–819. https://doi.org/10.1038/321817b0.
(31) Russell, B. C.; Croudace, I. W.; Warwick, P. E.; Milton, J. A. Determination of Precise 135Cs/137Cs Ratio in Environmental Samples Using Sector Field Inductively Coupled Plasma Mass Spectrometry. *Anal. Chem.* **2014**, *86* (17), 8719–8726. https://doi.org/10.1021/ac501894a.
(32) Zhu, L.; Hou, X.; Qiao, J. Determination of Ultralow Level 135Cs and 135Cs/137Cs Ratio in Environmental Samples by Chemical Separation and Triple Quadrupole ICP-MS. *Anal. Chem.* **2020**, *92* (11), 7884–7892. https://doi.org/10.1021/acs.analchem.0c01153.
(33) Yang, G.; Tazoe, H.; Yamada, M. 135Cs Activity and 135Cs/137Cs Atom Ratio in Environmental Samples before and after the Fukushima Daiichi Nuclear Power Plant Accident. *Sci Rep* **2016**, *6* (1), 24119. https://doi.org/10.1038/srep24119.
(34) Bu, W.; Tang, L.; Liu, X.; Wang, Z.; Fukuda, M.; Zheng, J.; Aono, T.; Hu, S.; Wang, X. Ultra-Trace Determination of the 135Cs/137Cs Isotopic Ratio by Thermal Ionization Mass Spectrometry with Application to Fukushima Marine Sediment Samples. *J. Anal. At. Spectrom.* **2019**, *34* (2), 301–309. https://doi.org/10.1039/C8JA00380G.
(35) Lee, T.; Teh-Lung, K.; Hsiao-Ling, L.; Ju-Chin, C. First Detection of Fallout Cs-135 and Potential Applications of 137Cs /135Cs Ratios. *Geochimica et Cosmochimica Acta* **1993**, *57*, 3493–3497. https://doi.org/10.1016/0016-7037(93)90555-B.
(36) Zheng, J.; Bu, W.; Tagami, K.; Shikamori, Y.; Nakano, K.; Uchida, S.; Ishii, N. Determination of 135Cs and 135Cs/137Cs Atomic Ratio in Environmental Samples by Combining Ammonium Molybdophosphate (AMP)-Selective Cs Adsorption and Ion-Exchange Chromatographic

Separation to Triple-Quadrupole Inductively Coupled Plasma–Mass Spectrometry. *Anal. Chem.* **2014**, *86* (14), 7103–7110. https://doi.org/10.1021/ac501712m.

(37) Dunne, J. A.; Richards, D. A.; Chen, H.-W. Procedures for Precise Measurements of 135Cs/137Cs Atom Ratios in Environmental Samples at Extreme Dynamic Ranges and Ultra-Trace Levels by Thermal Ionization Mass Spectrometry. *Talanta* **2017**, *174*, 347–356. https://doi.org/10.1016/j.talanta.2017.06.033.

(38) Ohno, T.; Muramatsu, Y. Determination of Radioactive Cesium Isotope Ratios by Triple Quadrupole ICP-MS and Its Application to Rainwater Following the Fukushima Daiichi Nuclear Power Plant Accident. *J. Anal. At. Spectrom.* **2014**, *29* (2), 347–351. https://doi.org/10.1039/C3JA50291K.

(39) Song, M.; Probst, Th. U.; Berryman, N. G. Rapid and Sensitive Determination of Radiocesium (Cs-135, Cs-137) in the Presence of Excess Barium by Electrothermal Vaporization-Inductively Coupled Plasma-Mass Spectrometry (ETV-ICP-MS) with Potassium Thiocyanate as Modifier. *Fresenius J Anal Chem* **2001**, *370* (6), 744–751. https://doi.org/10.1007/s002160000678.

(40) Russell, B. C.; Croudace, I. W.; Warwick, P. E. Determination of 135Cs and 137Cs in Environmental Samples: A Review. *Analytica Chimica Acta* **2015**, *890*, 7–20. https://doi.org/10.1016/j.aca.2015.06.037.

(41) Liezers, M.; Farmer, O. T.; Thomas, M. L. Low Level Detection of 135Cs and 137Cs in Environmental Samples by ICP-MS. *J Radioanal Nucl Chem* **2009**, *282* (1), 309. https://doi.org/10.1007/s10967-009-0227-z.

(42) Lehto, J.; Hou, X. *Chemistry and Analysis of Radionuclides: Laboratory Techniques and Methodology*; John Wiley & Sons, Ltd, 2010.

(43) Magre, A.; Boulet, B.; Pourcelot, L.; Roy-Barman, M.; de Vismes Ott, A.; Ardois, C. Improved Radiocesium Purification in Low-Level Radioactive Soil and Sediment Samples Prior to 135Cs/137Cs Ratio Measurement by ICP-MS/MS. *J Radioanal Nucl Chem* **2022**, *331* (9), 4067–4076. https://doi.org/10.1007/s10967-022-08413-y.

(44) Epov, V. N.; Taylor, V.; Lariviere, D.; Evans, R. D.; Cornett, R. J. Collision Cell Chemistry for the Analysis of Radioisotopes by Inductively Coupled Plasma Mass Spectrometry. *Journal of Radioanalytical and Nuclear Chemistry* **2003**, *258* (3), 473–480. https://doi.org/10.1023/B:JRNC.0000011740.95950.d9.

(45) Evrard, O.; Van Beek, P.; Gateuille, D.; Pont, V.; Lefèvre, I.; Lansard, B.; Bonté, P. Evidence of the Radioactive Fallout in France Due to the Fukushima Nuclear Accident. *Journal of Environmental Radioactivity* **2012**, *114*, 54–60. https://doi.org/10.1016/j.jenvrad.2012.01.024.

(46) Pourcelot, L.; Louvat, D.; Gauthier-Lafaye, F.; Stille, P. Formation of Radioactivity Enriched Soils in Mountain Areas. *Journal of Environmental Radioactivity* **2003**, *68* (3), 215–233. https://doi.org/10.1016/S0265-931X(03)00051-1.

(47) Roussel-Debel, S.; Renaud, P.; Métivier, J.-M. 137Cs in French Soils: Deposition Patterns and 15-Year Evolution. *Science of The Total Environment* **2007**, *374* (2), 388–398. https://doi.org/10.1016/j.scitotenv.2006.12.037.

(48) Evrard, O.; Chartin, C.; Laceby, J. P.; Onda, Y.; Wakiyama, Y.; Nakao, A.; Cerdan, O.; Lepage, H.; Jaegler, H.; Vandromme, R.; Lefèvre, I.; Bonté, P. Radionuclide Contamination in Flood Sediment Deposits in the Coastal Rivers Draining the Main Radioactive Pollution Plume of Fukushima Prefecture, Japan (2011–2020). *Earth System Science Data* **2021**, *13* (6), 2555–2560. https://doi.org/10.5194/essd-13-2555-2021.

(49) Duffa, C. Répartition du Plutonium et de l'Américium dans l'environnement terrestre de la basse vallée du Rhône., Aix Marseille III, 2001, thesis report.

(50) Duffa, C.; Renaud, P.; Calmet, D. Activités de 238Pu et de 239+240Pu dans les sols cultivés de la basse vallée du Rhône. *Comptes Rendus de l'Académie des Sciences - Series IIA - Earth and Planetary Science* **2001**, *332* (4), 275–281. https://doi.org/10.1016/S1251-8050(01)01522-1.

(51) Ballestra, S. B.; Holm, E.; Walton, A.; Whitehead, N. E. Fallout Deposition at Monaco Following the Chernobyl Accident. *Journal of Environmental Radioactivity* **1987**, *5* (5), 391–400. https://doi.org/10.1016/0265-931X(87)90013-0.
(52) Froidevaux, P.; Steinmann, P.; Pourcelot, L. Long-Term and Long-Range Migration of Radioactive Fallout in a Karst System. *Environ Sci Technol* **2010**, *44* (22), 8479–8484. https://doi.org/10.1021/es100954h.
(53) Bouisset, P.; Nohl, M.; Cossonnet, C.; Boulet, B.; Thomas, S.; Cariou, N.; Salaun, G. Contribution of Close-in Fallout from the French Atmospheric Tests in Inventories of 137Cs, 241Am and Plutonium (238, 239, 240) in Gambier Islands (French Polynesia) – Signatures of Stratospheric Fallout in the Southern Hemisphere. *Journal of Environmental Radioactivity* **2021**, *235–236*, 106624. https://doi.org/10.1016/j.jenvrad.2021.106624.
(54) Goutelard, F.; Morello, M.; Calmet, D. Alpha-Spectrometry Measurement of Am and Cm at Trace Levels in Environmental Samples Using Extraction Chromatography. *Journal of Alloys and Compounds* **1998**, *271–273*, 25–30. https://doi.org/10.1016/S0925-8388(98)00017-6.
(55) Chawla, F.; Steinmann, P.; Pfeifer, H.-R.; Froidevaux, P. Atmospheric Deposition and Migration of Artificial Radionuclides in Alpine Soils (Val Piora, Switzerland) Compared to the Distribution of Selected Major and Trace Elements. *Science of The Total Environment* **2010**, *408* (16), 3292–3302. https://doi.org/10.1016/j.scitotenv.2010.03.012.
(56) Bundt, M.; Albrecht, A.; Froidevaux, P.; Blaser, P.; Flühler, H. Impact of Preferential Flow on Radionuclide Distribution in Soil. *Environ. Sci. Technol.* **2000**, *34* (18), 3895–3899. https://doi.org/10.1021/es9913636.

SUPPORTING INFORMATION

Identification of the origin of radiocesium into the environment in areas remote from nuclear accident and military test sites using the $^{135}Cs/^{137}Cs$ isotopic signature

Anaelle Magre [a,b], Beatrice Boulet [a], Anne de Vismes Ott [a], Olivier Evrard [b], Laurent Pourcelot [c]*

[a] Laboratoire de métrologie de la radioactivité dans l'environnement (PSE-ENV/SAME/LMRE), IRSN, 91400 Orsay, France

[b] Laboratoire des Sciences du Climat et de l'Environnement (CNRS, CEA, UVSQ-IPSL), Université Paris-Saclay, 91191 Gif-sur-Yvette, France

[c] Laboratoire d'étude et d'expertise sur la radioactivité de l'environnement (PSE-ENV/SEREN/LEREN), IRSN, 13108 Saint-Paul-lez-Durance, France

[*]*Email: laurent.pourcelot@irsn.fr*

Number of pages in Supporting Information section: 5, including cover.

Number of Tables: 4

Table S1: Characteristics of the lake sediment and soil samples investigated

Sample name	Study area	Sampling site	Latitude *(°)*	Longitude *(°)*	Sampling date	Matrix	Depth *(cm)*
20_PNM45_1	Mercantour mountain	Terre Rouge Main lake	44.18089	7.18554	04/11/2020	Lake sediment	—
20_PNM45_2		Terre Rouge Temporary lake	—	—	04/11/2020	Lake sediment	—
20_PNM45_3		Superior Lausfer lake	44.22139	7.08944	05/11/2020	Lake sediment	—
20_PNM45_4		Inferior Lausfer lake	44.22052	7.0876	05/11/2020	Lake sediment	—
13_PNM4		Cerise lake	44.13538	7.39015	24/09/2013	Lake sediment	—
13_PNM7		Besson lake	44.1387	7.32004	25/09/2013	Lake sediment	—
13_PNM9		Vens lake	44.31122	6.93234	09/10/2023	Lake sediment	—
13_PNM19		Lausfer lake	44.2214	7.08668	11/10/2013	Lake sediment	—
21_PNM24_5		Terre Rouge Main lake	44.190413	7.18485	16/06/2021	Lake sediment	—
21_PNM24_6		Terre Rouge Inferior lake	44.18946	7.183011	16/06/2021	Lake sediment	—
21_PNM24_1	Mercantour moutain	Restefond pass	44.344317	6.849132	15/06/2021	Surface soil Subsurface soil	0 – 5 5 – 10
21_PNM24_2		Restefond pass	44.344260	6.849150	15/06/2021	Surface soil	0 – 5
21_PNM24_3		Restefond pass	43.341771	6.848091	15/06/2021	Surface soil Subsurface soil	0 – 5 5 – 10
21_PNM24_4		Restefond pass	43.341771	6.848091	15/06/2021	Surface soil Subsurface soil	0 – 5 5 – 10
14_PYR_2	Pyrenees	Coumebière plateau	42.78271	1.38986	25/06/2014	Surface soil	0 – 10
14_PYR_3		Labant pond	42.77735	1.39279	25/06/2014	Surface soil Subsurface soil	0 – 10 10 – 20
14_PYR_53		Besse pass	42.9697	-0.46900	08/10/2014	Surface soil	0 – 10

Table S2 : ICP-MS/MS parameters for $^{135}Cs/^{137}Cs$ isotopic ratio measurement

Parameters	Settings
Sample introduction	
Sample uptake	80 s (0.30 rps)
Stabilization time	40 s
Probe rinse	20 s (0.30 rps)
Spectrum acquisition	
Integration time	1 s for m/z = 115 and 138 5 s for m/z 135 and 137
Q2 peak pattern	3 points
Replicates	5
Sweeps/replicates	1000
Plasma	
RF power	1550 W
RF matching	1.27 V
Sample Depth	5.4 mm
Nebulizer gas	1.11 $L.min^{-1}$
Option gas	0.0 %
Nebulizer pump	0.10 rps
S/C temperature	2 °C
Makeup gas	0.00 $L.min^{-1}$
Lenses	
Extract 1	-19.0 V
Extract 2	-235.0 V
Omega bias	-110 V
Omega lens	12.0 V
Q1 entrance	2.0 V
Q1 exit	2.0 V
Cell focus	3.0 V
Cell entrance	-50 V
Cell exit	-58 V
Deflect	1.0 V
Plate bias	-50 V
Q1	
Q1 bias	-1.0 V
Q1 prefilter bias	-8.5 V
Q1 postfilter bias	-10.0 V
Cell	
He flow	1 $mL.min^{-1}$
3^{rd} gas flow	NH_3/He – 48% (4.79 $mL.min^{-1}$)
4^{th} gas flow	N_2O – 52 % (0.55 $mL.min^{-1}$)
OctP bias	-4.0 V
Axial acceleration	2.0 V
OctP RF	160 V
Energy discrimination	-7.0 V

Table S3: Analytical performance (Cs recovery and eluate purity) achieved for each sample analyzed

Sample name	Depth *(cm)*	Analyzed mass *(g)*	^{137}Cs recovery *(%)*	Interferent concentration in the ICP-MS measurement fraction *(ng.g^{-1})*			
				Ba	Mo	Sb	Sn
20_PNM45_1	—	63.142	83	1.09 ± 0.01	0.57 ± 0.02	0.11 ± 0.01	1.85 ± 0.02
20_PNM45_2	—	61.519	73	1.69 ± 0.03	0.28 ± 0.02	0.08 ± 0.01	1.25 ± 0.03
20_PNM45_3	—	94.853	78	1.52 ± 0.31	0.41 ± 0.09	0.08 ± 0.02	2.89 ± 0.59
20_PNM45_4	—	102.059	62	1.39 ± 0.67	17.46 ± 2.29	0.04 ± 0.02	0.24 ± 0.14
13_PNM4	—	113.369	76	1.96 ± 0.29	0.24 ± 0.03	0.06 ± 0.01	2.17 ± 0.28
13_PNM7	—	84.482	84	1.20 ± 0.19	0.28 ± 0.04	0.46 ± 0.07	1.67 ± 0.27
13_PNM9	—	60.080	84	1.15 ± 0.02	0.21 ± 0.02	0.05 ± 0.01	1.14 ± 0.01
13_PNM19	—	80.360	80	1.02 ± 0.19	0.39 ± 0.07	0.21 ± 0.04	0.81 ± 0.15
21_PNM24_5	—	99.030	77	1.16 ± 0.36	0.29 ± 0.09	0.08 ± 0.02	2.24 ± 0.66
21_PNM24_6	—	49.671	82	2.10 ± 0.02	2.45 ± 0.04	0.07 ± 0.01	1.48 ± 0.02
21_PNM24_1	0 – 5	5.131	82	0.24 ± 0.01	1.88 ± 0.04	0.04 ± 0.01	3.01 ± 0.08
	5 – 10	6.326	85	0.37 ± 0.02	0.94 ± 0.11	0.04 ± 0.01	12.16 ± 0.63
21_PNM24_2	0 – 5	109.884	57	3.39 ± 0.11	11.43 ± 0.28	0.03 ± 0.01	0.48 ± 0.03
21_PNM24_3	0 – 5	10.852	83	0.60 ± 0.01	0.18 ± 0.02	0.04 ± 0.01	7.21 ± 0.84
	5 – 10	55.037	82	5.45 ± 0.88	0.26 ± 0.04	0.05 ± 0.01	0.47 ± 0.08
21_PNM24_4	0 – 5	11.970	93	0.09 ± 0.01	0.13 ± 0.01	0.05 ± 0.01	5.64 ± 0.12
	5 – 10	100.610	71	1.03 ± 0.02	0.33 ± 0.02	0.07 ± 0.01	1.04 ± 0.02
14_PYR_2	0 – 10	113.455	65	0.34 ± 0.01	0.31 ± 0.02	0.07 ± 0.01	0.62 ± 0.03
14_PYR_3	0 – 10	34.039	72	0.52 ± 0.01	0.38 ± 0.02	0.04 ± 0.01	1.48 ± 0.02
	10 – 20	103.584	61	1.76 ± 0.03	0.31 ± 0.01	0.04 ± 0.01	1.21 ± 0.04
14_PYR_53	0 – 10	110.342	68	3.39 ± 0.01	0.30 ± 0.01	0.03 ± 0.01	0.77 ± 0.02

Table S4: Estimation of the $^{135}Cs/^{137}Cs$ ratio characterizing NWT fallout by weighting the proportions of annual deposits with the theorical isotopic ratio of 1 at the time of detonation.

Year	Annual deposition* (10^{16} Bq)		Proportion of annual deposition (%)	Theoretical $^{135}Cs/^{137}Cs$ isotopic ratio per year** (decay corrected to January 1st, 2022)
	^{90}Sr	^{137}Cs		
Pre-1958	6.68	10.69	14.54	4.57
1958	2.33	3.73	5.07	4.37
1959	3.89	6.22	8.47	4.27
1960	0.97	1.55	2.11	4.17
1961	1.30	2.08	2.83	4.08
1962	5.34	8.54	11.62	3.98
1963	9.70	15.52	21.11	3.89
1964	6.13	9.81	13.34	3.80
1965	2.86	4.58	6.23	3.72
1966	1.21	1.94	2.63	3.63
1967	0.62	0.99	1.35	3.55
1968	0.72	1.15	1.57	3.47
1969	0.54	0.86	1.18	3.39
1970	0.76	1.22	1.65	3.31
1971	0.70	1.12	1.52	3.24
1972	0.32	0.51	0.70	3.16
1973	0.12	0.19	0.26	3.09
1974	0.45	0.72	0.98	3.02
1975	0.22	0.35	0.48	2.95
1976	0.10	0.16	0.22	2.89
1977	0.30	0.48	0.65	2.82
1978	0.37	0.59	0.81	2.76
1979	0.2	0.32	0.44	2.69
1980	0.11	0.18	0.24	2.63
TOTAL	45.94	73.50	100	3.97

**Annual ^{137}Cs deposition estimated from the annual ^{90}Sr deposition from NWT reported in the UNSCEAR report (1982) and the average $^{137}Cs/^{90}Sr$ activity ratio of 1.6.*

***$^{135}Cs/^{137}Cs$ isotopic ratio calculated per year assuming a $^{135}Cs/^{137}Cs$ isotopic ratio of 1 at the time of detonation and for decay-correction to January 1st, 2022. The total corresponds to the $^{135}Cs/^{137}Cs$ characteristic of NWT weighted by the proportion of annual deposits.*